Supporting Material for

A Refined Reaction-Diffusion Model of Tau-Microtubule Dynamics and Its Application in FDAP Analysis

Maxim Igaev,[1]* Dennis Janning,[1] Frederik Sündermann,[1] Benedikt Niewidok,[1] Roland Brandt,[1] Wolfgang Junge[2]

[1]Department of Neurobiology and Department of Biophysics[2], University of Osnabrück, Osnabrück, Germany
*Correspondence: maxim.igaev@biologie.uni-osnabrueck.de

Photoactivation profiles. Sharp axial borders versus Gaussian profile

To derive the solutions to Eqs. 2 and 5 one needs to define the initial conditions for [TF](z,t=0) and [TB](z,t=0). These are given by the fluorescence distribution along the cellular process directly after photoactivation (photoactivation profile). In the experiment the laser flash creates a Gaussian photoactivation profile with a characteristic length 2σ. However, a profile with sharp axial borders (i.e. when the fluorescence is constant in $z\in[-\sigma,\sigma]$ and abruptly goes to zero beyond this range) serves as a good approximation as validated by subsidiary numerical simulations employing the *Freefem++* partial differential equation solver (53). More specifically, two types of photoactivation profiles were tested: a cylindrical profile with sharp axial borders

$$\begin{aligned}[\mathrm{TF}](z,t=0) &= \begin{cases}[\mathrm{TF}]_{eq}, & \text{if} \quad |z|\le\sigma,\\ 0, & \text{elsewhere},\end{cases}\\ [\mathrm{TB}](z,t=0) &= \begin{cases}[\mathrm{TB}]_{eq}, & \text{if} \quad |z|\le\sigma,\\ 0, & \text{elsewhere},\end{cases}\end{aligned} \tag{S.1}$$

and a profile where the fluorescence intensity along the axial line had a slightly modified Gaussian distribution

$$\begin{aligned}[\mathrm{TF}](z,t=0) &= [\mathrm{TF}]_{eq}\exp(-2z^2/\sigma^2),\\ [\mathrm{TB}](z,t=0) &= [\mathrm{TB}]_{eq}\exp(-2z^2/\sigma^2).\end{aligned} \tag{S.2}$$

The recording profile was the same in both cases, namely, a cylinder of diameter $2R$ and of characteristic length 2σ. The FDAP curves for both cases were calculated for a wide range of parameters and compared by calculating the sum of squared residuals which did not exceed the value of 10^{-2}.

Calculation of the validity areas for the system Eq. 2

To define parametric borders where one approximation can be considered as being valid and another as invalid, we calculated their areas of validity as follows. For each of the special cases the respective FDAP transient was calculated. The value D was fixed and the reaction rates were varied over a wide range (from 10^{-4} to 10^{4}) on a log scale. Each FDAP was sampled over M = 112 time intervals, and the mean-square deviation from the full numerical

solution (res^2) was calculated as $res^2 = \sum_{i=1}^{M}\left[FDAP_{simplified}(t_i) - FDAP_{full}(t_i)\right]^2$. A deviation less than 0.01 was considered as acceptable. The validity of the simplified solutions was also confirmed by Monte Carlo simulations of FDAP transients and subsequent fitting by the respective approximations (see the section *Monte Carlo simulations* further and Fig. S1).

FDAP fitting and error analysis

Analysis of FDAP transients was performed with self-written *python*-based routines (54). The routines included three blocks. The first block served for the numerical Laplace inversion of the full models and the simplified regimes for a given set of the system parameters. For the inversion we made use of the algorithm developed in (55). This algorithm is relatively simple and produces accurate transforms for Laplace functions of different complexity. The second block of the routines corresponded to the least square analysis. For this we used a simple brute-force mapping procedure to approximately minimize the χ^2-value in the parametric space Π, i.e.

$$\chi^2(\boldsymbol{\beta}) = \sum_{i=1}^{n}\left[\frac{f(t_i) - FDAP(t_i,\boldsymbol{\beta})}{\sigma(t_i)}\right]^2, \quad \text{(S.3)}$$

$$\min_{\boldsymbol{\beta}\in\Pi}\chi^2(\boldsymbol{\beta}) \to \boldsymbol{\beta}^*, \quad \text{(S.4)}$$

where $f(t)$ represents the average of several experimental curves sampled in a time set $\{t_i\}$ together with its standard deviation $\sigma(t)$, $FDAP(t,\boldsymbol{\beta})$ is a desired theoretical curve also sampled in $\{t_i\}$, and $\boldsymbol{\beta}$ is an arbitrary vector from Π. The minimization procedure consisted in ordered discretization of the parametric space and subsequent finding a vector $\boldsymbol{\beta}^*$ that minimizes χ^2-value in Eq. S.3. The discretization of the (k^*_{on}, k_{off})-plane was always done with a 0.01 increment on a log scale. The diffusion constant space was discretized with a 0.01 increment on a linear scale. We also used parallel computing tools to reduce the total calculation time.

To compute 95% confidence intervals of the estimated parameters $\boldsymbol{\beta}^*$ we employed the formulae for the nonlinear data fitting given in (56). The algorithm consisted of the following steps 1) finding $\boldsymbol{\beta}^*$ which approximately minimizes the χ^2-value in Eq. S.3, 2) calculating residuals between $f(t)$ and the desired theoretical curve as follows $res_i = [f(t_i) - FDAP(t_i,\boldsymbol{\beta}^*)]/\sigma(t_i)$, 3) calculating the degrees of freedom, df, as $df = n - n_p - 1$, where n is the number of time steps, and n_p is the number of fitting parameters, 4) calculating the estimated residual variance as $s^2 = ||\mathbf{res}||^2/df$, 5) calculating the estimated coefficient variance as $\mathbf{V} = s^2(\mathbf{J}^T\,\mathbf{J})^{-1}$, where $J_{ij} = \partial FDAP(t_i,\boldsymbol{\beta})/\partial\beta_j$ is the Jacobian and the indices i and j denote the time index and the parameter index within $\boldsymbol{\beta}$, respectively. Finally, the upper and lower confidence bounds were calculated as $\pm(\mathbf{D}_V)^{1/2}\,F^{-1}(0.95 \mid df)$, where $F^{-1}(p \mid k)$ is the inverse of the Student's t-cumulative distribution function with k degrees of freedom and the corresponding probability p, and $\mathbf{D}_V$ a vector composed of the diagonal elements of $\mathbf{V}$. The calculation of the confidence intervals, as well as subsidiary operations, was implemented in the third block of the routines.

Derivation of the general solution to the reaction-diffusion system Eq. 2

Equation 2 describes the diffusion and first-order-reaction kinetics of a molecule (here tau) in a homogeneous cylindrical space. We assume that the diffusion is restricted to the free state.

Before the activating laser flash is fired, there is no tau fluorescence, tau is in equilibrium with its binding sites in the photoactivation region, and its concentrations in the free, $[TF]_{eq}$, and bound, $[TB]_{eq}$, states are equilibrium concentrations. The laser flash activates a subset of molecules that is then detectable. At the initial moment (directly after the photoactivation) the concentrations of visible free, $[TF](z,t=0)$, and bound, $[TB](z,t=0)$, molecules within the photoactivation region $z \in [-\sigma, \sigma]$ become $[TF]_{eq}$ and $[TB]_{eq}$, respectively, and remain zero elsewhere. A standard way of finding analytical solutions of partial differential equations for non-periodic problems like Eq. 2 is an integral transform, e.g., the Laplace transform, i.e. $\overline{f}(p) = \int_0^\infty f(t)\exp(-pt)dt$, where $f(t)$ is an arbitrary function defined for all real non-negative numbers $t \geq 0$ and $\overline{f}(p)$ is a function of a complex argument p. In the Laplace space linear differential operators turn to algebraic operations. This reduces the system of partial differential equations to a system of ordinary differential equations. The inverse Laplace transform of the final solution yields the desired time function but may not always be readily derived.

Applying the Laplace transform to Eq. 2 and bearing in mind the initial conditions yield

$$p\overline{[TF]} = D\frac{\partial^2\overline{[TF]}}{\partial z^2} - k^*_{on}\overline{[TF]} + k_{off}\overline{[TB]} + [TF](z, t=0), \quad \text{(S.5)}$$

$$p\overline{[TB]} = k^*_{on}\overline{[TF]} - k_{off}\overline{[TB]} + [TB](z, t=0). \quad \text{(S.6)}$$

By rearranging the terms in Eq. S.6 and substituting the expression for $\overline{[TB]}$ into Eq. S.5 we obtain

$$\frac{\partial^2\overline{[TF]}}{\partial z^2} - q^2\overline{[TF]} = -V(z), \quad \text{(S.7)}$$

where $q^2 = (p/D)(1 + k^*_{on}/(k_{off} + p))$ and $V(z) = ([TF](z,t=0)/D)(1 + k^*_{on}/(k_{off} + p))$. In the most general case Eq. S.7 represents the standard inhomogeneous Helmholtz equation that frequently occurs in problems of mathematical physics. In a simple one-dimensional case it could also describe a driven harmonic oscillator without damping. It is intuitively obvious that the solution to Eq. S.7 should have exponentially decaying tails as $|z| \to +\infty$ and be continuously symmetrical everywhere in the real one-dimensional coordinate space with respect to the point $z = 0$. It should also contain a particular solution within the photoactivation region. Hence, we attempt a solution of the following form

$$\overline{[TF]}(z, p) = \frac{V}{q^2} + C_1\left(\exp(-qz) + \exp(qz)\right), \quad |z| \leq \sigma, \quad \text{(S.8)}$$

$$\overline{[TF]}(z, p) = C_2\exp(-q|z|), \quad |z| > \sigma, \quad \text{(S.9)}$$

where the constants C_1 and C_2 are to be determined using the requirement that the function $\overline{[TF]}(z,p)$ together with its first spatial derivative must be continuous everywhere on the Oz axis and particularly at $z = \pm\sigma$. This requirement yields

$$C_1 = -\frac{V}{2q^2}\exp(-q\sigma) = -\frac{[TF]_{eq}}{2p}\exp(-q\sigma), \quad \text{(S.10)}$$

$$C_2 = \frac{V}{2q^2}(\exp(q\sigma) - \exp(-q\sigma)) = \frac{[TF]_{eq}}{2p}(\exp(q\sigma) - \exp(-q\sigma)). \quad \text{(S.11)}$$

Hereafter, we compute the expression for the averaged intensity within the photoactivation region. The Laplace image is then as follows

$$\overline{FDAP}(p) = \left\langle \overline{[\mathrm{TF}]}(z,p) + \overline{[\mathrm{TB}]}(z,p) \right\rangle, \quad \text{(S.12)}$$

where $<\ldots> \equiv (1/2\sigma)\int_{-\sigma}^{\sigma}\ldots dz$ is the spatial average over the photoactivation region. The only term in Eq. S.12 that has to be averaged is $\overline{[\mathrm{TF}]}(z,p)$ as the expression for $\overline{[\mathrm{TB}]}(z,p)$ can be easily expressed in terms of $\overline{[\mathrm{TF}]}(z,p)$ from Eq. S.6. Thus, it is sufficient to calculate $\left\langle \overline{[\mathrm{TF}]}(z,p) \right\rangle$:

$$\left\langle \overline{[\mathrm{TF}]}(z,p) \right\rangle = \frac{1}{2\sigma}\int_{-\sigma}^{\sigma}\left[\frac{[\mathrm{TF}]_{eq}}{p} - \frac{[\mathrm{TF}]_{eq}}{2p}\exp(-q\sigma)\big(\exp(-qz)+\exp(qz)\big)\right]dz = \frac{[\mathrm{TF}]_{eq}}{p} - \frac{[\mathrm{TF}]_{eq}}{2p}\frac{1-\exp(-2q\sigma)}{q\sigma} \quad \text{(S.13)}$$

and to then substitute it into Eq. S.12. Hence, one obtains Eq. 4 (see the main text).

Derivation of the simplified solutions

Here we discuss the simplified regimes arising when restrictions on the parameters D, σ, k^*_{on} and k_{off} are imposed. The derivations partly resemble those in (18, 19), except that the geometry of the problem under consideration is one-dimensional.

Pure diffusion

Pure diffusion denotes the case when the concentration of free molecules is much larger than that of bound molecules, i.e., $[\mathrm{TF}]_{eq} >> [\mathrm{TB}]_{eq}$. This assumption imposes limitations on the on- and off-rates as follows from Eq. 3, namely, $k^*_{on}/k_{off} << 1$. Hence, Eq. 4 transforms to

$$\overline{FDAP}_{pure}(p) \approx \frac{1}{p} - \frac{1-\exp(-2\sqrt{p\sigma^2/D})}{2p\sqrt{p\sigma^2/D}}. \quad \text{(S.14)}$$

Equation S.14 can now be inverted analytically to yield the real time FDAP,

$$FDAP_{pure}(t) \approx erf\sqrt{\frac{\tau_D}{t}} + \sqrt{\frac{t}{\pi\tau_D}}\left(\exp\left(-\frac{\tau_D}{t}\right)-1\right), \quad \text{(S.15)}$$

where $\tau_D = \sigma^2/D$ is the characteristic diffusion time of a molecule over the photoactivation region.

Effective diffusion

When the average time before a molecule is bound while diffusing across the photoactivation region is much shorter than τ_D, i.e., $1/k^*_{on} << \tau_D$, the system can be considered as being in the *effective diffusion* mode. It has been shown in (18) that by introducing a new variable $p' = p\,\tau_D(1 + k^*_{on}/k_{off}) = p\,\tau_{eff}$ and redefining $\overline{FDAP}_{new}(p) = \overline{FDAP}(p)/\tau_{eff}$, the full numerical solution can be reduced to one similar to the pure diffusion case but with the characteristic

time equal to τ_{eff}. Doing so in case of Eq. 4 results in

$$FDAP_{eff}(t) \approx erf\sqrt{\frac{\tau_{eff}}{t}} + \sqrt{\frac{t}{\pi\tau_{eff}}}\left(\exp\left(-\frac{\tau_{eff}}{t}\right)-1\right). \quad \text{(S.16)}$$

Reaction dominant

A constraint diametrically opposite to the previous one brings us to a regime called *reaction dominant*. In this regime τ_D is much shorter than the average association time of a molecule, i.e., $1/k^*_{on} >> \tau_D$. Diffusion and binding act on different time scales and are hence separable. We thus decompose Eq. 4 into

$$\overline{FDAP}_{reaction}(p) = [\mathrm{TF}]_{eq}\overline{FDAP}_{pure}(p) + \overline{FDAP}_{dissoc}(p). \quad \text{(S.17)}$$

The expression for $\overline{FDAP}_{dissoc}(p)$ can be found as a limiting case of Eq. 4 when $\sigma\to 0$, that is,

$$\overline{FDAP}_{dissoc}(p) = \lim_{\sigma\to 0}\overline{FDAP}(p) = \frac{[\mathrm{TB}]_{eq}}{p + k_{off}}. \quad \text{(S.18)}$$

It reflects a FDAP signal which is strongly governed by the dissociation rate of molecules. The Laplace transform is then easily found:

$$FDAP_{reaction}(t) \approx [\mathrm{TF}]_{eq}FDAP_{pure}(t) + [\mathrm{TB}]_{eq}\exp(-k_{off}t). \quad \text{(S.19)}$$

Hybrid behaviour

Sprague et al. (18) have also found a somewhat intermediate solution between the effective diffusion and reaction dominant regimes where the majority of molecules are bound ($k^*_{on}/k_{off} >> 1$) but diffusion and binding act on a comparable time scale ($1/k^*_{on} \sim \tau_D$). Applying the same procedure to Eq. 4 we obtain

$$\overline{FDAP}_{hybrid}(p) \approx \frac{1}{p + k_{off}}\left(\frac{k_{off}}{p}\left(1 - \frac{1-\exp(-2q\sigma)}{2q\sigma}\right)+1\right), \quad \text{(S.20)}$$

where $(q\sigma)^2 \approx k^*_{on}\tau_D p/(p + k_{off})$.

Derivation of the solution to the diffusing-bound-state model

Equation 5 also describes diffusion and first-order-reaction kinetics of a species in a homogeneous cylindrical space. However, there is non-zero diffusion in both free and bound states. The initial conditions are the same as for the system Eq. 2 (see the derivation above). Applying the same strategy for finding the solution to Eq. 5 one obtains

$$\frac{\partial^2\overline{[\mathrm{TF}]}}{\partial z^2} - q^2\overline{[\mathrm{TF}]} + \eta^2\overline{[\mathrm{TB}]} = -V_1(z), \quad \text{(S.21)}$$

$$\frac{\partial^2\overline{[\mathrm{TB}]}}{\partial z^2} + \varphi^2\overline{[\mathrm{TF}]} - \psi^2\overline{[\mathrm{TB}]} = -V_2(z), \quad \text{(S.22)}$$

where the parameters $q^2 = (p + k^*_{on})/D_F$, $\eta^2 = k_{off}/D_F$, $\varphi^2 = k^*_{on}/D_B$, $\psi^2 = (p + k_{off})/D_B$, $V_1(z) = c(z,t=0)/D_F$, and $V_2(z) = s(z,t=0)/D_B$. The particular solution within the photoactivation region can be found by setting the derivatives in Eqs. S.21 and S.22 to zero, hence

$$\overline{[\mathrm{TF}]}_{part} = \frac{\psi^2 V_1 + \eta^2 V_2}{q^2\psi^2 - \varphi^2\eta^2}, \text{ (S.23)}$$

$$\overline{[\mathrm{TB}]}_{part} = \frac{\varphi^2 V_1 + q^2 V_2}{q^2\psi^2 - \varphi^2\eta^2}, \text{ (S.24)}$$

within the photoactivation region and zero elsewhere. We then consider the homogeneous problem to Eqs. S.21 and S.22

$$\frac{\partial^2\overline{[\mathrm{TF}]}}{\partial z^2} = q^2\overline{[\mathrm{TF}]} - \eta^2\overline{[\mathrm{TB}]}, \text{ (S.25)}$$

$$\frac{\partial^2\overline{[\mathrm{TB}]}}{\partial z^2} = -\varphi^2\overline{[\mathrm{TF}]} + \psi^2\overline{[\mathrm{TB}]}. \text{ (S.26)}$$

This is a simple matrix ordinary differential equation with the defining matrix **A** composed of the constant coefficients on the right sides of Eqs. S.25 and S.26. The fundamental solution to this system can be given in terms of the eigenvalues and eigenvectors of **A** (57), namely

$$\begin{pmatrix}\overline{[\mathrm{TF}]}(z,p)\\ \overline{[\mathrm{TB}]}(z,p)\end{pmatrix} = M_1\left(\exp(-\lambda_1 z) + \exp(\lambda_1 z)\right)\mathbf{G}_1 + M_2\left(\exp(-\lambda_2 z) + \exp(\lambda_2 z)\right)\mathbf{G}_2, \quad |z| \le \sigma, \text{ (S.27)}$$

$$\begin{pmatrix}\overline{[\mathrm{TF}]}(z,p)\\ \overline{[\mathrm{TB}]}(z,p)\end{pmatrix} = N_1\exp(-\lambda_1|z|)\mathbf{G}_1 + N_2\exp(-\lambda_2|z|)\mathbf{G}_2, \quad |z| > \sigma, \text{ (S.28)}$$

where $M_{1,2}$ and $N_{1,2}$ are arbitrary constants to be found by using the matching condition at $z = \pm\sigma$. The eigenvalues $\lambda_{1,2}$ and the eigenvectors $\mathbf{G}_{1,2}$ of the matrix **A** are expressed as follows

$$\mathbf{G}_{1,2} = \begin{pmatrix}1\\ \dfrac{\lambda_{2,1}^2 - \psi^2}{\eta^2}\end{pmatrix}, \text{ (S.29)}$$

$$\lambda_{1,2}^2 = \frac{q^2 + \psi^2 \pm \sqrt{(q^2 - \psi^2)^2 + 4\eta^2\varphi^2}}{2}, \text{ (S.30)}$$

Combined with the partial solutions, Eqs. S.23 and S.24, and averaged over the photoactivation region according to Eq. S.12, the Laplace transform for the FDAP signal generalizes to Eq. 6, whereby

$$A(p) = \frac{\lambda_1^2 - q^2 - \eta^2}{\lambda_1^2 - \lambda_2^2}\left(\frac{\lambda_2^2 - q^2}{\eta^2}\overline{[\mathrm{TF}]}_{part} + \overline{[\mathrm{TB}]}_{part}\right), \text{ (S.31)}$$

$$B(p) = \frac{\lambda_2^2 - q^2 - \eta^2}{\lambda_1^2 - \lambda_2^2}\left(\frac{\lambda_1^2 - q^2}{\eta^2}\overline{[\mathrm{TF}]}_{part} + \overline{[\mathrm{TB}]}_{part}\right). \text{ (S.32)}$$

Now let us show that the *pure* and *effective diffusion* approximations are still applicable despite non-zero diffusion of molecules in the bound state. In case of *pure diffusion* the derivation is trivial. Indeed, since the majority of molecules are free and only infrequently interact with their binding sites, one can eliminate the reaction terms on the right side of Eq. 5. FDAPs are now to be found separately for the free (fast) and bound (slow) fractions. The resulting FDAP is then as follows

$$FDAP_{pure}(t) = [\mathrm{TF}]_{eq}\,FDAP_F(t) + [\mathrm{TB}]_{eq}\,FDAP_B(t), \text{ (S.33)}$$

where $FDAP_{F,B}(t)$ are given by Eq. S.15 with the diffusion constants exchanged by D_F and D_B, respectively. Bearing in mind that the *pure diffusion* approximation is valid only when

$[TF]_{eq} >> [TB]_{eq}$, Eq. S.33 simplifies even more, namely to

$$FDAP_{pure}(t) \approx FDAP_F(t). \quad \text{(S.34)}$$

Note the difference between Eqs. S.33 and a simple two-component expression

$$FDAP_{pure}(t) = \rho FDAP_F(t) + (1-\rho) FDAP_B(t), \quad \text{(S.35)}$$

where ρ and 1-ρ are the fractions of molecules diffusing in the states TF and TB, respectively. In this case ρ is an independent fit parameter and does not depend on the reaction rates. Equation S.35 hence cannot be reduced to Eq. S.34 since the species TF and TB diffuse independently.

In case of *effective diffusion* the binding equilibrium establishes instantaneously so that it can be assumed $[TB] \approx (k^*_{on}/k_{off})[TF]$ for every time moment at every spatial position in the medium. Merging Eqs. 5A and 5B and expressing [TB] in terms of [TF] as mentioned before, one obtains

$$\frac{\partial [TF]}{\partial t} \approx \frac{D_F + (k^*_{on}/k_{off}) D_B}{1 + k^*_{on}/k_{off}} \nabla^2 [TF], \quad \text{(S.36)}$$

where the value before $\nabla^2 c$ is constant and now considered as an effective diffusion coefficient. The resulting FDAP is then given by Eq. S.16 with the only difference being the new effective diffusion constant from Eq. S.36.

Monte Carlo simulations

(a) To ensure the absence of the longitudinal diffusion inhibition by the MT network we simulated the diffusion of tau by Monte Carlo simulations. The simulation space was defined as a tube of radius R = 500 nm. The tube was not restricted in the axial direction. MT packing was provided by N_{MT} parallel MTs, each of radius R_{MT} = 12.5 nm (as depicted in Fig. 2, middle), with the MT-MT distance ($R_{MT\text{-}MT}$) equal to ~70 nm. The number of MTs, and therewith the volume fill factor φ, was varied but did not exceed the percolation threshold set by the effective medium approach (φ = 0.5). At the initial moment (t = 0), 1000 particles were randomly placed within the photoactivation region of 4 µm in length (σ = 2 µm) so that none of them was in the MT phase. Once the MT topology and the molecular ensemble were set, the time loop was started. The time step, Δt, was equal to 1 µs. At each time step displacements Δx, Δy and Δz for each particle were generated as normally distributed random numbers with the standard deviation equal to $\sqrt{2D\Delta t}$. Reflection boundary conditions at the outer boundary of the simulation space as well as at the MT surface were imposed. The abovementioned procedure was iterated for 30×10^6 time steps (30 s).

(b) We also performed Monte Carlo simulations to validate the simplified solutions to the kinetic model (Eq. 2). We assumed a homogeneous distribution of tau-binding sites (see Fig. 2, left). While defining the molecular ensemble at t = 0, each particle had a probability $k^*_{on}/(k^*_{on} + k_{off})$ of being bound and a probability $k_{off}/(k^*_{on} + k_{off})$ of being free. At each time step, each free particle could bind with a probability $1 - \exp(-k^*_{on}\Delta t)$, and each bound particle could unbind with a probability $1 - \exp(-k_{off}\Delta t)$. Once the free and bound populations were defined, the random displacements Δx, Δy and Δz for the free population were generated. Reflection boundary conditions only at the outer boundary were imposed. The procedure was again iterated for 100×10^6 time steps (100 s). The simulations were repeated for different (k^*_{on}, k_{off}) values.

In both cases the normalized FDAP for each time step signal was calculated by counting the number of particles within the photoactivation region, $z \in [-\sigma, \sigma]$, and normalizing

it to the total number of particles.

Calculation of the volume fill factor of MTs

We calculated the upper bond for the volume fill factor of MTs (each of radius R_{MT}), φ_{max}, packed in a cylindrical cellular process with a circular cross-section (of radius R). Due to the parallel orientation of MTs within the cellular process, the 3D problem is equivalent to a 2D packing problem, where the goal is to arrange N_{MT} circles in a larger circle so that their common radius is maximal. Solutions to this problem have been computed for various N_{MT} (58, 59). One important parameter, while computing the optimal packing, is the density α, i.e. the ratio of total area occupied by the small circles to that of the larger one. Since in our case the radius of MTs is fixed, one needs to rescale α with respect to the actual area occupied by a MT cross-section in order to relate it to the volume fill factor of MTs. Hence,

$$\varphi_{\max} = \alpha \frac{R_{MT}^2}{R_{MT-MT}^2}, \quad \text{(S.37)}$$

where $R_{MT\text{-}MT}$ is the minimal separation between the MT centers.

Supporting Figures

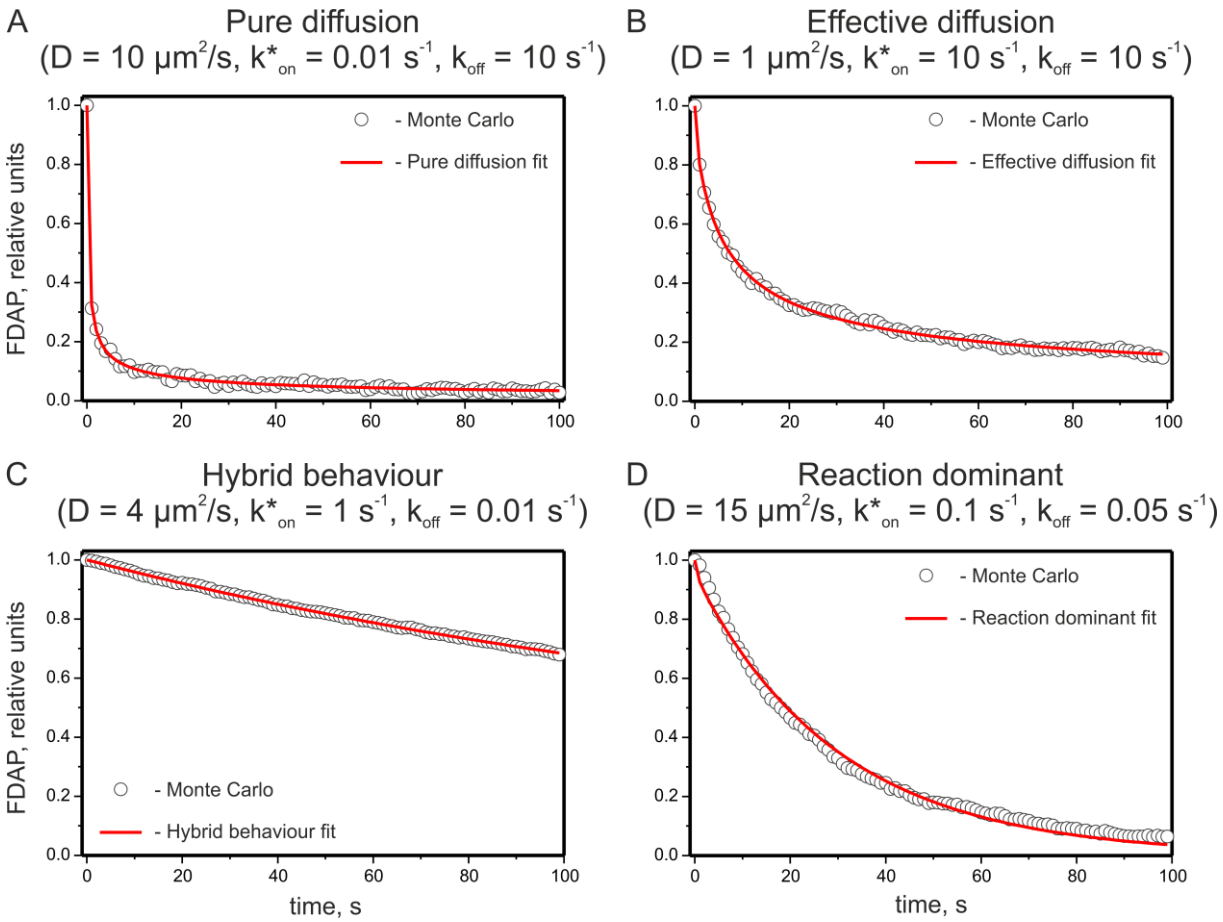

FIGURE S1 Validation of the simplified solutions through Monte Carlo simulations of FDAP transients. Numerically simulated FDAP curves (*gray circles*, σ = 2 μm) were fitted by each of the simplified solutions from Table 1. For *pure diffusion* and *effective diffusion* there was only one fit parameter, namely D ($D_{eff} = D/(1 + k^*_{on}/k_{off})$ in case of *effective diffusion*) that was varied. For *hybrid behaviour* and *reaction dominant* the parameter D was fixed while fitting, and only the reaction constants were varied. As expected, each FDAP

transient was well described only by the approximation of the same name. Fits are depicted with *red lines*. (*A*) The FDAP transient was computed so that $k^*_{on} << k_{off}$, which corresponded to *pure diffusion*. The *pure diffusion* fit resulted in $D \approx 10.7$ μm^2/s. (*B*) The FDAP transient was computed so that $\tau_D >> 1/k^*_{on}$, which corresponded to *effective diffusion*. The *effective diffusion* fit resulted in $k^*_{on}/k_{off} \approx 1.02$. (*C*) The FDAP transient was computed so that $\tau_D \sim 1/k^*_{on}$ but $k^*_{on} >> k_{off}$, which corresponded to *hybrid behaviour*. The *hybrid behaviour* fit resulted in $k^*_{on} \approx 0.8$ s^{-1} and $k_{off} \approx 0.009$ s^{-1}. (*D*) The FDAP transient was computed so that $\tau_D << 1/k^*_{on}$, which corresponded to *reaction dominant*. The *reaction dominant* fit resulted in $k^*_{on} \approx 0.22$ s^{-1} and $k_{off} \approx 0.03$ s^{-1}.

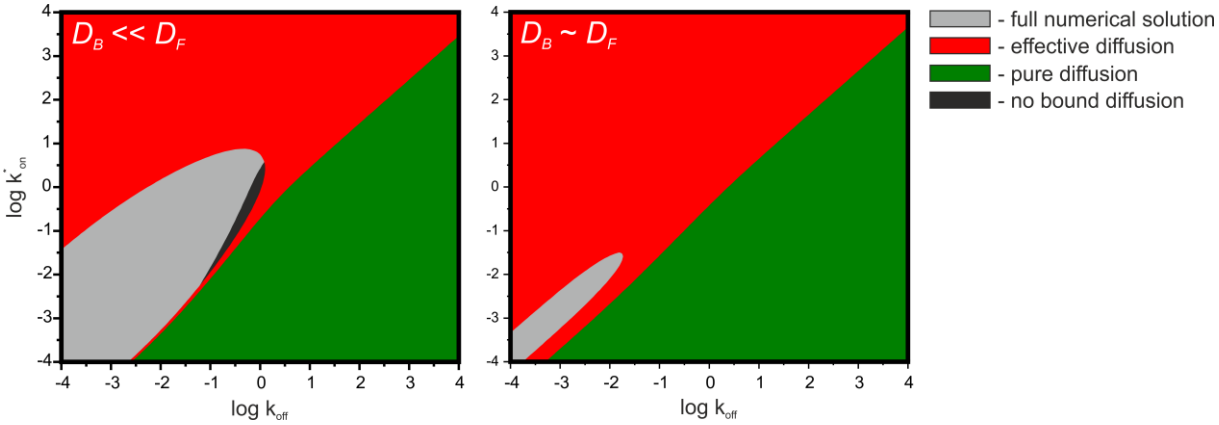

FIGFURE S2 Superposition of the validity areas of the simplified solutions to the diffusing-bound-state model. (*A*) A parametric area (*black*) was found where the full numerical solution of Eq. 2 (no bound diffusion) can well approximate the diffusing-bound-state model (see the discussion section for details). The *pure* and *effective diffusion* validity areas cover a considerable part of the (k^*_{on}, k_{off})-space even at small values of D_F (D_F = 10 μm^2/s, D_B = 0.3 μm^2/s, σ = 2 μm). (B) The area assigned to the full numerical solution of Eq. 2 vanishes with the increase of D_B. On the contrary, the coverage of the parametric space by the pure and effective diffusion validity areas increases as D_B approaches D_F (D_F = 10 μm^2/s, D_B = 7 μm^2/s, σ = 2 μm).

Supporting References

53. Hecht, F. 2012. New development in freefem++. J. Numer. Math. 20: 251–265.

54. Oliphant, T.E. 2007. Python for Scientific Computing. Comput. Sci. Eng. 9: 10–20.

55. Valsa, J., and L. Brančik. 1998. Approximate formulae for numerical inversion of Laplace transforms. Int. J. Numer. Model. Electron. Networks, Devices Fields. 11: 153–166.

56. Bates, D.M., and D.G. Watts. 1988. Nonlinear Regression Analysis and Its Applications. Hoboken, NJ, USA: John Wiley & Sons, Inc.

57. Moya-Cessa, H.M., and F. Soto-Eguibar. 2011. Differential Equations: An Operational Approach. Rinton Press, New Jersey.

58. Lubachevsky, B., and R. Graham. 1997. Curved hexagonal packings of equal disks in a circle. Discrete Comput. Geom. 194: 179–194.

59. Graham, R.L., B.D. Lubachevsky, K.J. Nurmela, and P.R.J. Östergård. 1998. Dense packings of congruent circles in a circle. Discrete Math. 181: 139–154.